A Non-Radical Mechanism for Methane Hydroxylation at the Diiron Active Site of Soluble Methane Monooxygenase

Kazunari Yoshizawa* and Takashi Yumura[a]

Abstract: We propose a non-radical mechanism for the conversion of methane into methanol by soluble methane monooxygenase (sMMO), the active site of which involves a diiron active center. We assume the active site of the $MMOH_Q$ intermediate, exhibiting direct reactivity with the methane substrate, to be a bis(μ-oxo)diiron(IV) complex in which one of the iron atoms is coordinatively unsaturated (five-coordinate). Is it reasonable for such a diiron complex to be formed in the catalytic reaction of sMMO? The answer to this important question is positive from the viewpoint of energetics in density functional theory (DFT) calculations. Our model thus has a vacant coordination site for substrate methane. If $MMOH_Q$ involves a coordinatively unsaturated iron atom at the active center, methane is effectively converted into methanol in the broken-symmetry singlet state by a non-radical mechanism; in the first step a methane C–H bond is dissociated via a four-centered transition state (TS1) resulting in an important intermediate involving a hydroxo ligand and a methyl ligand, and in the second step the binding of the methyl ligand and the hydroxo ligand through a three-centered transition state (TS2) results in the formation of a methanol complex. This mechanism is essentially identical to that of the methane–methanol conversion by the bare FeO^+ complex and relevant transition metal–oxo complexes in the gas phase. Neither radical species nor ionic species are involved in this mechanism. We look in detail at kinetic isotope effects (KIEs) for H atom abstraction from methane on the basis of transition state theory with Wigner tunneling corrections.

Keywords: alkane hydroxylation · C–H bond activation · density functional calculations · kinetic isotope effect · methane monooxygenase

Introduction

Methane monooxygenase (MMO) catalyzes the transformation of methane and dioxygen into methanol and water at ambient pressure and temperature [Eq. (1)].[1]

$$CH_4 + NADH + H^+ + O_2 \rightarrow CH_3OH + NAD^+ + H_2O \quad (1)$$

This reaction is the essential first step in the metabolic pathway for the consumption of methane by methanotrophic bacteria. Since methane is an inert hydrocarbon, the ability of MMO to facilitate the conversion of methane into methanol under physiological conditions has fascinated many researchers and led them to investigate potential applications of its catalytic function.[1] Soluble MMO (sMMO) is purified from *Methylococcus capsulatus* (Bath) and *Methylosinus trichosporium* OB3b, and consists of three protein components: a dimeric $\alpha_2\beta_2\gamma_2$ hydroxylase (MMOH), an NADH-dependent [Fe_2S_2] and FAD-containing reductase (MMOR), and a regulatory protein (MMOB).[2] In MMOH each α subunit contains a carboxylate-bridged diiron center as the active site for dioxygen activation and methane hydroxylation.[3] The structure of MMOH is altered through interactions with MMOB, which lead to changes in the kinetics and the regiospecificity in the catalysis of MMOH.[4] From X-ray crystallographic analyses, the two iron atoms have octahedral environments in the resting state of MMOH, with the oxidation states of [$Fe^{III}Fe^{III}$] ($MMOH_{ox}$).[3d,e] The diiron(III) enzyme is reduced to the [$Fe^{II}Fe^{II}$] state ($MMOH_{red}$) by electrons provided from a reductase protein MMOR[5] (Scheme 1).[6, 7] Upon reduction of the oxidized diiron(III) enzyme, a carboxylate shift of Glu243 occurs at the active center of the reduced diiron(II) enzyme, to render the iron atoms five-coordinate.[3d–f] After the formation of the [$Fe^{II}Fe^{II}$] complex, molecular oxygen is bound to the vacant coordination site of the diiron active center. The first spectroscopically observed intermediate is $MMOH_{peroxo}$.[6] The $MMOH_{peroxo}$ intermediate subsequently converts into the high-valent [$Fe^{IV}Fe^{IV}$] intermediate ($MMOH_Q$), which can be monitored

[a] Prof. K. Yoshizawa, T. Yumura[+]
Institute for Fundamental Research of Organic Chemistry
Kyushu University
Fukuoka 812-8581 (Japan)
Fax: (+81) 92-642-2735
E-mail: kazunari@ms.ifoc.kyushu-u.ac.jp

[+] Visiting graduate student at Kyushu University, from the Department of Molecular Engineering, Kyoto University (Japan)

Supporting information for this article is available on the WWW under http://www.chemeurj.org or from the author.

 DOI: 10.1002/chem.200204269

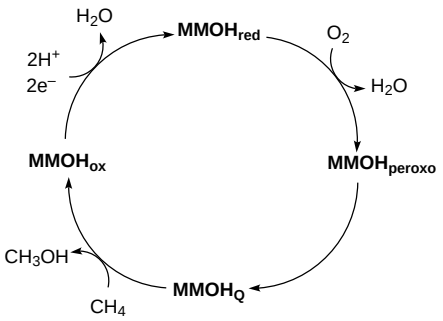

Scheme 1. Proposed reaction cycle for MMOH.

by stopped-flow spectroscopy, thanks to its bright yellow color.[6, 7] Intermediate $MMOH_Q$ has a direct reactivity toward substrate methane. From a combined Mössbauer–EXAFS investigation, Que, Lipscomb, and co-workers suggested that the active site of $MMOH_Q$ should involve a bis(μ-oxo)diiron(IV) core,[8] in which the two iron atoms are antiferromagnetically coupled.[7b] Although X-ray structural analyses for this important intermediate have not yet been successful, the EXAFS investigation suggested that the coordination number of the iron atoms is no greater than five.[8]

An important mechanistic question with respect to the catalytic cycle of MMOH is how the bis(μ-oxo)diiron(IV) core of the $MMOH_Q$ active site oxidizes methane into methanol. One possible mechanism for hydroxylation by MMOH is a radical rebound mechanism, widely believed to occur in the hydroxylation mechanism of cytochrome P450,[9] the active site of which involves a mononuclear iron–oxo species with a porphyrin ring as a ligand. In the first step of this mechanism, a homolytic cleavage of a C–H bond of substrate alkane leads to a radical intermediate, and in the second step the resultant alkyl radical moves to the newly formed OH group, resulting in the formation of an alcohol complex.[10] However, Newcomb and Lippard et al. have suggested, from experiments with radical-clock substrate probes, that a measured lifetime of a putative radical species in MMOH catalysis is shorter than $\approx$150 fs, which is inconsistent with the formation of a discrete radical species.[11, 12] A similarly short lifetime for the radical species was also observed in the hydroxylation of chiral ethane on MMOH.[13] Despite many experimental investigations, the mechanism of the C–H bond activation of methane in the catalytic function of sMMO is still under debate.

Recent density functional theory (DFT) calculations have provided useful information on the veiled methane hydroxylation by $MMOH_Q$.[14–16] As shown in Scheme 2a, a C–H bond of methane is believed to be cleaved in a homolytic manner by the coordinatively saturated diiron model complex of $MMOH_Q$ in very high-spin states such as nonet and undecet.[14c,e, 15] After the dissociation of a C–H bond of methane, the resultant methyl radical is shifted to the formed OH group as in Scheme 2a, which requires an activation energy of about 3–7 kcal mol^{-1}. These studies demonstrated that sMMO-mediated hydroxylation reactions proceed along the lines that the radical rebound mechanism suggests. On the other hand (Scheme 2b), the methyl radical is proposed to recombine with an iron center through a weak Fe–CH_3 bond after the H atom abstraction.[14a] In contrast to the radical rebound mechanism, the conversion of methane into methanol by $MMOH_Q$ is proposed to occur by a non-synchronous concerted mechanism (Scheme 2c).[1h, 16] After the homolytic cleavage of a C–H bond of methane in this mechanism, methanol is formed in a nearly barrierless fashion.[16b] The presence of the radical rebound and the non-synchronous concerted mechanisms may explain the experimental results obtained for the chiral ethane hydroxylation on MMOH.[16b] Recently, Friesner et al. estimated 69–84% retention of stereochemistry for the hydroxylation of a chiral ethane on MMOH, from a semiclassical molecular dynamics (MD) simulation involving a mixture of non-synchronous, concerted and bound radical trajectories.[16d]

As shown in Scheme 2d, we have proposed that methane can be hydroxylated by a non-radical mechanism if one of the iron atoms at the active site of $MMOH_Q$ is coordinatively unsaturated.[17] In this mechanism, an iron atom that is coordinatively unsaturated and has a vacant coordination site for substrate is responsible for methane activation and hydroxylation. Experimental and theoretical studies[18, 19] of methane hydroxylation by the bare FeO^+ complex may give a hint as to the mechanism of sMMO-mediated methane hydroxylation. Schwarz, Schröder, and co-workers have made detailed studies of the methane to methanol conversion by FeO^+—formed from the reaction between Fe^+ and pulsed-in N_2O under Fourier transform ion cyclotron resonance (FTICR) conditions—and proposed that the complex HO-Fe^+-CH_3 is involved in the hydroxylation reaction as a central

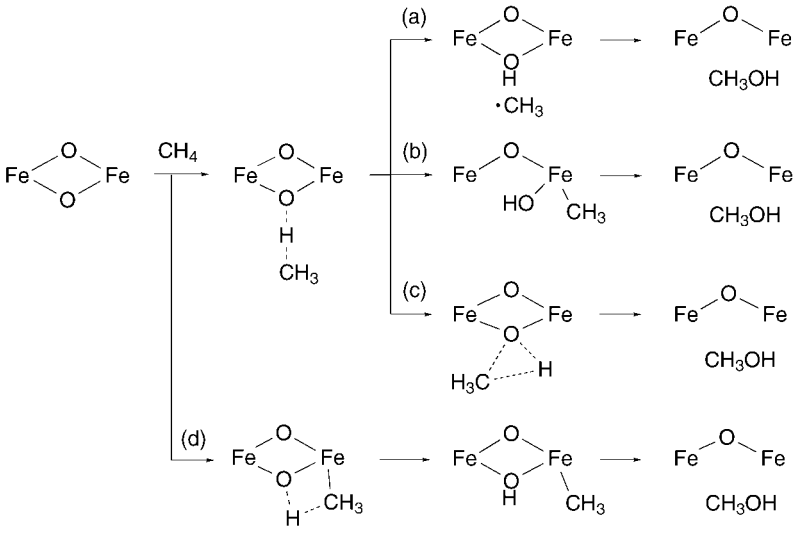

Scheme 2. Possible pathways for methane hydroxylation by $MMOH_Q$.

intermediate.[18] We have investigated the mechanism and energetics of the methane–methanol conversion by FeO^+ and by other cationic transition metal-oxo species by DFT calculations and proposed that the reaction should occur in a two-step manner (Scheme 3).[19]

The first step is the C–H bond dissociation, which occurs through a four-centered transition state with an Fe–C bond (TS1), and the second step is the binding of the resultant methyl ligand and the hydroxo ligand (TS2). These chemical processes take place on a single iron atom. A striking feature of this mechanism is that neither radical species nor ionic species are involved in the course of the hydroxylation reaction, because the methyl moiety formed as a result of the C–H bond dissociation coordinates directly to the iron atom. This non-radical mechanism is applicable to sMMO-mediated methane hydroxylation if $MMOH_Q$ involves a coordinatively unsaturated iron atom at the active center. Using small bis(μ-oxo)diiron(IV) models with a bridging formate and three OH or H_2O ligands, we have proposed that methane hydroxylation should take place without involvement of radical species, as in Scheme 3.

Our previous MMO models were too small to represent the coordination sphere around the diiron active site of $MMOH_Q$, although the actual coordination sphere remains unknown, especially about the coordination number that we are interested in. Recently, Friesner, Lippard, and co-workers proposed that a large-scale calculation works well in predicting reasonable values for the activation energy in the catalytic cycle of MMOH.[16a–c] Morokuma et al., using the ONIOM approach, suggested that local structures of the active site of MMOH are controlled by protein environments.[15h] In this paper, with the aid of a reasonable model of the active site of $MMOH_Q$, we show how methane can be converted into methanol in a two-step, non-radical mechanism. The rational improvement of the model should increase the reliability of the non-radical mechanism for methane hydroxylation by $MMOH_Q$. We also analyze kinetic isotope effects (KIEs) for the H atom abstraction from methane on the basis of transition state theory with tunneling corrections. Since the KIE is an important measure in discussion of how an H atom is abstracted from methane by the active species of $MMOH_Q$, comparison of KIEs obtained from experimental[5e, 6e, 20] and from computational approaches should shed new light on the black-box reaction by $MMOH_Q$.

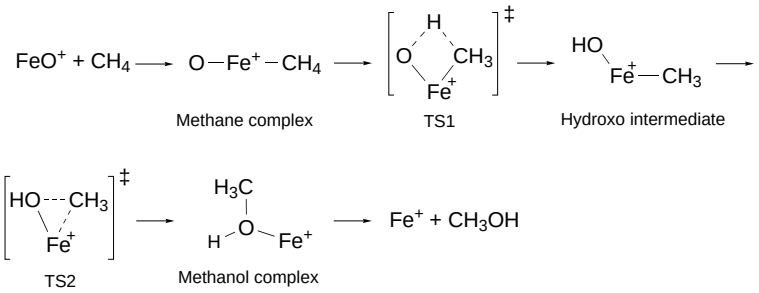

Scheme 3. Proposed two-step mechanism of methane–methanol conversion by FeO^+ and by other cationic transition-metal–oxo species.

Calculation methods: To calculate the observed antiferromagnetic states of the diiron complexes of $MMOH_{peroxo}$ and $MMOH_Q$[6, 7] we used the broken-symmetry methodology[21] throughout this study. This method is based on unrestricted Hartree–Fock or DFT calculations for spin-singlet open-shell systems in which spin-up and spin-down electrons are allowed to localize on different atomic centers. The broken-symmetry state is not a pure spin state described by a single determinant, but rather a weighted average of pure spin states to give a spin-coupling pattern with such an antiferromagnetic alignment. The energy of such a broken-symmetry state is usually above—but close to—the true ground-state energy.[21] This methodology has successfully been used to describe transition metal systems, including a large number of magnetically coupled centers in metalloproteins.[22–31] For example, Bencini et al. used the Xα method with the broken-symmetry approach to study dihalide,[22a] carbonato,[22b] and oxo-bridged Cu^{II} dinuclear complexes and a $Cu^{II}–V^{IV}$ heterodinuclear system.[22c] Stranger et al. calculated potential energy curves for face-shared $M_2Cl_9^{-3}$ and edged-shared $M_2Cl_{10}^{-4}$ bimetallic systems (M = Cr, Mo, and W) by using the broken-symmetry approximate density functional theory.[24] Alvarez et al. evaluated the magnetic coupling constants in hydroxo-, alkoxo-, oxo-, oxalato-, oxamidato-, and azido-bridged Cu^{II} dinuclear complexes by DFT methods and demonstrated that a combination of the hybrid Hartree–Fock/DFT B3LYP method with the broken-symmetry approach is the most successful strategy and provides results that are in good agreement with experimental data.[25] The broken-symmetry approach can thus correctly model the antiferromagnetic states in magnetically coupled systems, and it is consequently accepted as a good representation of the non-orthogonal, natural magnetic orbitals in dinuclear complexes. Taking cognizance of its limitations, we used this method to elucidate essential electronic features of the diiron complexes of MMOH.

Siegbahn,[14e] Friesner et al.,[16] and Noodleman et al.[26f,g,i] used the broken-symmetry approach to describe the electronic structures of the weakly coupled diiron active site of MMOH. If the active site of $MMOH_Q$ involves a kind of edge-shared six-coordinate diiron(IV) complex, this electronic feature is basically as described in Scheme 4.[24e–g] When an iron atom is octahedrally coordinated, the relevant d orbitals are split into three low-lying t_{2g} orbitals and two high-lying e_g orbitals. Thus, the low-lying and high-lying blocks at the diiron active center consist of six "t_{2g}" and four "e_g" orbitals, respectively. In the presence of excess spin-up or spin-down electron densities, spin-polarization causes a splitting of the d blocks (Scheme 4). If the iron–iron interaction is weak, each iron-based electron remains substantially localized on one iron atom and the other. The broken-symmetry approach always describes states in the weakly coupled limit, and the spin singlet ground state arises through antiparallel

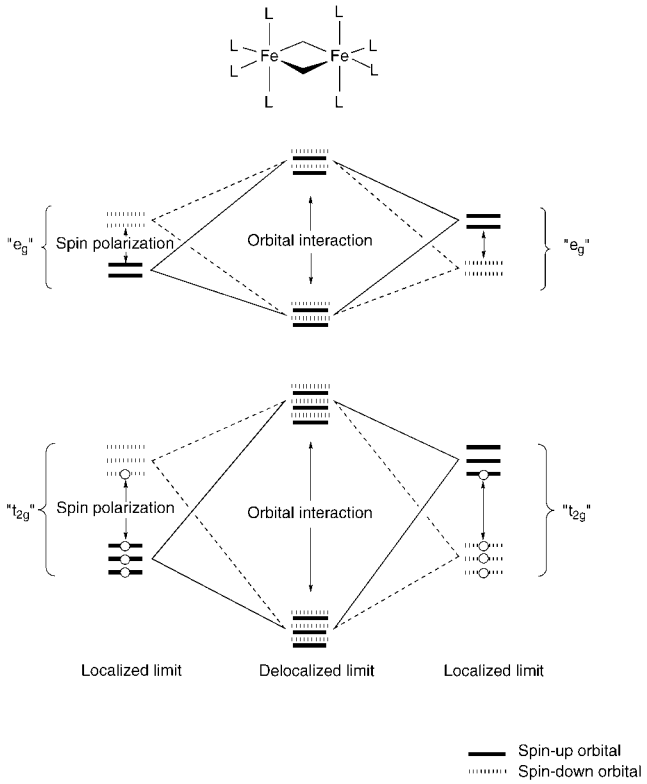

Scheme 4. The broken-symmetry state of an edge-shared diiron model complex. Bold lines indicate the energy levels of orbitals filled by spin-up electrons and hashed lines those of orbitals filled by spin-down electrons. The electronic configuration in the weakly coupled (localized) limit is shown at both sides and that in the strongly-coupled (delocalized) limit is shown at the center.

coupling of the spins on opposite centers. The broken-symmetry approach is usually more time-consuming than the usual spin-unrestricted approach in which the numbers of spin-up and spin-down electrons are different.

We carried out quantum-chemical calculations by the B3LYP method[32, 33] available on the Gaussian 98 ab initio program package.[34] This hybrid method consists of the Slater exchange, the Hartree–Fock exchange, Becke's exchange functional,[32] the correlation functional of Lee, Yang, and Parr (LYP),[33] and the correlation functional of Vosko, Wilk, and Nusair (VWN).[35] We optimized the reactants, products, and intermediates corresponding to potential energy minima and the transition states corresponding to saddle points and systematically computed harmonic vibrational frequencies to confirm that each optimized geometry corresponds to a local minimum possessing only real frequencies or a saddle point possessing only one imaginary frequency. We used the triple-zeta-valence (TZV) basis set[36] for the Fe and O atoms on the bis(μ-oxo)diiron(IV) core and substrate methane and the 3-21G basis set[37–39] for the other H, C, N, and O atoms modeling the amino acid residues around the diiron active site.

Results and Discussion:

A possible model of $MMOH_Q$: Siegbahn[14] and Morokuma et al.[15] adopted the nonet and undecet spin states for the diiron model complexes for the active site of $MMOH_Q$, on the assumption that the electronic structures of the antiferromagnetic and ferromagnetic states are essentially similar because the magnetic coupling between the two iron atoms is weak. Their DFT calculations demonstrated that the bridging oxygen atoms in the bis(μ-oxo)diiron(IV) complexes have significant spin densities in the high-spin states. Our B3LYP calculations showed that the spin densities on the bridging oxygen atoms are 0.7–0.8 in the nonet and undecet states. It is therefore reasonable to consider that, in these high-spin states, a C–H bond of methane is directly cleaved in a homolytic manner by the bridging oxygen atoms of the bis(μ-oxo)diiron(IV) core. Is this situation correct in the singlet state? We have paid great attention to an experimental fact that the unpaired spins on the two iron atoms are antiferromagnetically coupled in $MMOH_Q$,[7b] and in view of this we first optimized the coordinatively saturated diiron model complex in the broken-symmetry singlet state, as shown in the left of Figure 1. B3LYP calculations predict that the singlet state[40] is 1.6 kcal mol^{-1} less stable than the nonet state[41] adopted in earlier calculations. Since the B3LYP method tends to overestimate the stability of high-spin states, we also calculated the energy difference between the singlet state and the nonet state by the other DFT methods BLYP[32a, 33] and BPW91,[32a, 42] which correctly predict relative energies of states differing in spin multiplicity.[43] BLYP and BPW91 calculations correctly predict that the singlet state lies 15.2 and 16.6 kcal mol^{-1}, respectively, below the nonet state, as listed in Table 1, which indicates that the two iron centers of the dinuclear complex are antiferromagnetically coupled, consistently with experiment.[7b] It is therefore reasonable to consider how methane hydroxylation occurs on the singlet potential energy surface.

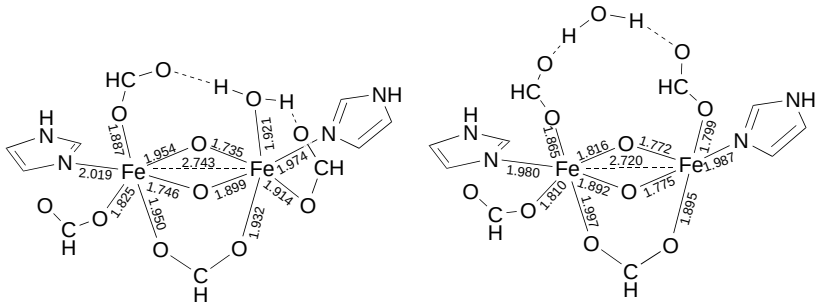

Figure 1. Optimized geometries of coordinatively saturated and unsaturated diiron model complexes as models of the active site of $MMOH_Q$. The formate and imidazole ligands used here mimic actual glutamate and histidine ligands, respectively. Bond lengths are in Å.

The spin densities on the iron atoms presented in Figure 2 are 1.6 and −1.7 in the diiron model complex (^{1}A) at the B3LYP level, these values being in good agreement with those calculated by Siegbahn.[14e] This is a reasonable result. If the

Table 1. Computed energy splittings between the ^{1}A state and the ^{9}A state for the saturated model of $MMOH_Q$ at various DFT levels. The geometry was fully optimized at each level of theory.

	E (^{1}A) [au]	E (^{9}A) [au]	ΔE [kcal mol^{-1}]
B3LYP	– 3956.73869709	– 3956.74126953	1.6
BLYP	– 3956.58710359	– 3956.56280894	– 15.2
BPW91	– 3956.91100266	– 3956.88446625	– 16.6

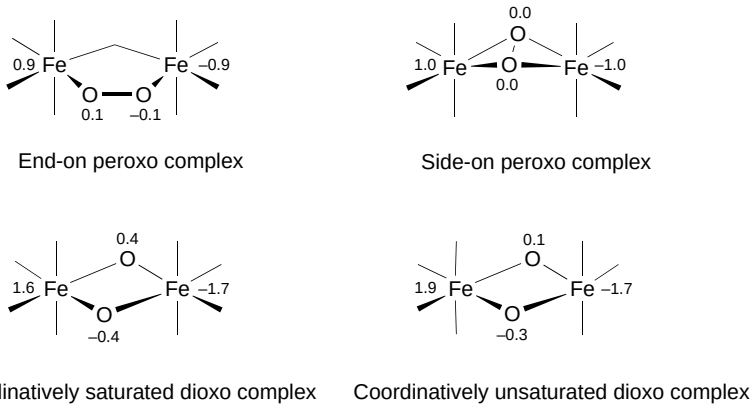

Figure 2. Calculated atomic spin densities for diiron model complexes of $MMOH_{peroxo}$ and $MMOH_Q$ at the B3LYP/(TZV + 3–21G) level of theory.

separation between the "e_g" and "t_{2g}" blocks is large enough, the low-lying "t_{2g}" block should be occupied by eight d electrons in the coordinatively saturated bis(μ-oxo)diiron(IV) complex. As shown in Scheme 4, three spin-up and one spin-down electrons are housed on the left-hand iron center, and one spin-up and three spin-down electrons are housed on the right-hand iron center. In contrast to the high-spin states, the calculated spin densities on the bridging oxygen atoms are 0.4 and -0.4 in the broken-symmetry singlet state. Although the magnetic coupling between the two iron atoms in the diiron complex is weak, the spin density distribution is of course different in the broken-symmetry singlet state and in the high-spin states, especially in the bridging oxygen atoms. In view of this result, we think that a C–H bond of methane is not effectively cleaved by the bridging oxygen atoms in the singlet state. We tried in vain to optimize the transition state for direct H atom abstraction in the broken-symmetry singlet state.

For the current study, we set up a new diiron model complex, shown on the right-hand side of Figure 1, in which one of the iron atoms is coordinatively unsaturated (five-coordinate). The water ligand is released from the right-hand iron atom of the coordinatively saturated diiron model, to be weakly bound to the two formate ligands through hydrogen bonds. Thus, one iron atom in our model of the $MMOH_Q$ active site is five-coordinate and the other one remains six-coordinate. Accordingly, the ligands of the two iron atoms on the right-hand side of Figure 1 are four formate and two imidazole ligands. Our model of $MMOH_Q$, consisting of 41 atoms, is essentially identical to that of Siegbahn.[14e] The shift of the water ligand in the six-coordinate diiron complex costs 32.4 kcal mol^{-1}, but this energetically unfavorable situation can be stabilized in energy when the protein environment is taken into account. The Fe–O distances in the coordinatively unsaturated diiron model were calculated to be 1.772, 1.775, 1.816, and 1.892 Å, which are in good agreement with those estimated from EXAFS measurements.[8] The diiron model has an Fe–Fe separation of 2.720 Å. Although this value is somewhat larger than the experimentally determined one (2.46 Å),[8] it is close to those calculated by Friesner et al.[16b] and by Siegbahn.[14e] Our model of $MMOH_Q$ is also supported by a recent proposal by Noodleman et al. that the hydrogen bond framework can create "open" coordination sites in the active site of $MMOH_Q$.[26i] In the optimized geometry of the coordinatively unsaturated diiron complex,[44] the spin densities on the iron atoms are 1.9 and -1.7, and those on the bridging oxygen atoms are 0.1 and -0.3 (Figure 2). Because this model involves a coordinatively unsaturated iron–oxo species, it can directly interact with substrate methane at the five-coordinate iron center. We think that methane hydroxylation can proceed in this model by the non-radical mechanism in which an H atom of methane is abstracted via the four-centered transition state while the Fe–C bond is kept.[17, 19]

Is such a bis(μ-oxo)diiron(IV) complex—in which one of the iron atoms is five-coordinate—formed in the catalytic reaction of MMOH? This is an important question to be addressed in this article. For this purpose we first paid special attention to the catalytic cycle in the region between $MMOH_{red}$ and $MMOH_Q$. In the course of the reaction, dioxygen is incorporated into the diiron active site of $MMOH_{red}$, which results in the formation of $MMOH_{peroxo}$ and $MMOH_Q$. Dioxygen binding was suggested to take place by substitution of the weakly coordinating water distal to the two histidine residues.[1h, 3e] According to the observed X-ray structure of $MMOH_{red}$,[3e] we assumed that a five-coordinate diiron complex should be generated before dioxygen binding to the diiron active site of $MMOH_{red}$. As shown in Figure 3, a formate ligand forms a bidentate chelating interaction with the left-hand iron atom and a single bond with the right-hand iron atom in the optimized geometry of the model complex of the $MMOH_{red}$ active site. The Fe–Fe distance was calculated to be 3.559 Å. Since each iron atom has a five-coordination environment, the diiron complex has a vacant coordination site for the binding of dioxygen.

After dioxygen binding to the active site of $MMOH_{red}$, a transient peroxo intermediate $MMOH_{peroxo}$, in which the two iron atoms are antiferromagnetically coupled,[6a] is generated in the reaction pathway. We considered and performed calculations for two kinds of peroxo complexes to model $MMOH_{peroxo}$ by the broken-symmetry approach (Figure 3). One is an end-on peroxo complex with a *cis*-μ-1,2 bridging mode, and the other is a side-on peroxo complex with a μ-η^2:η^2

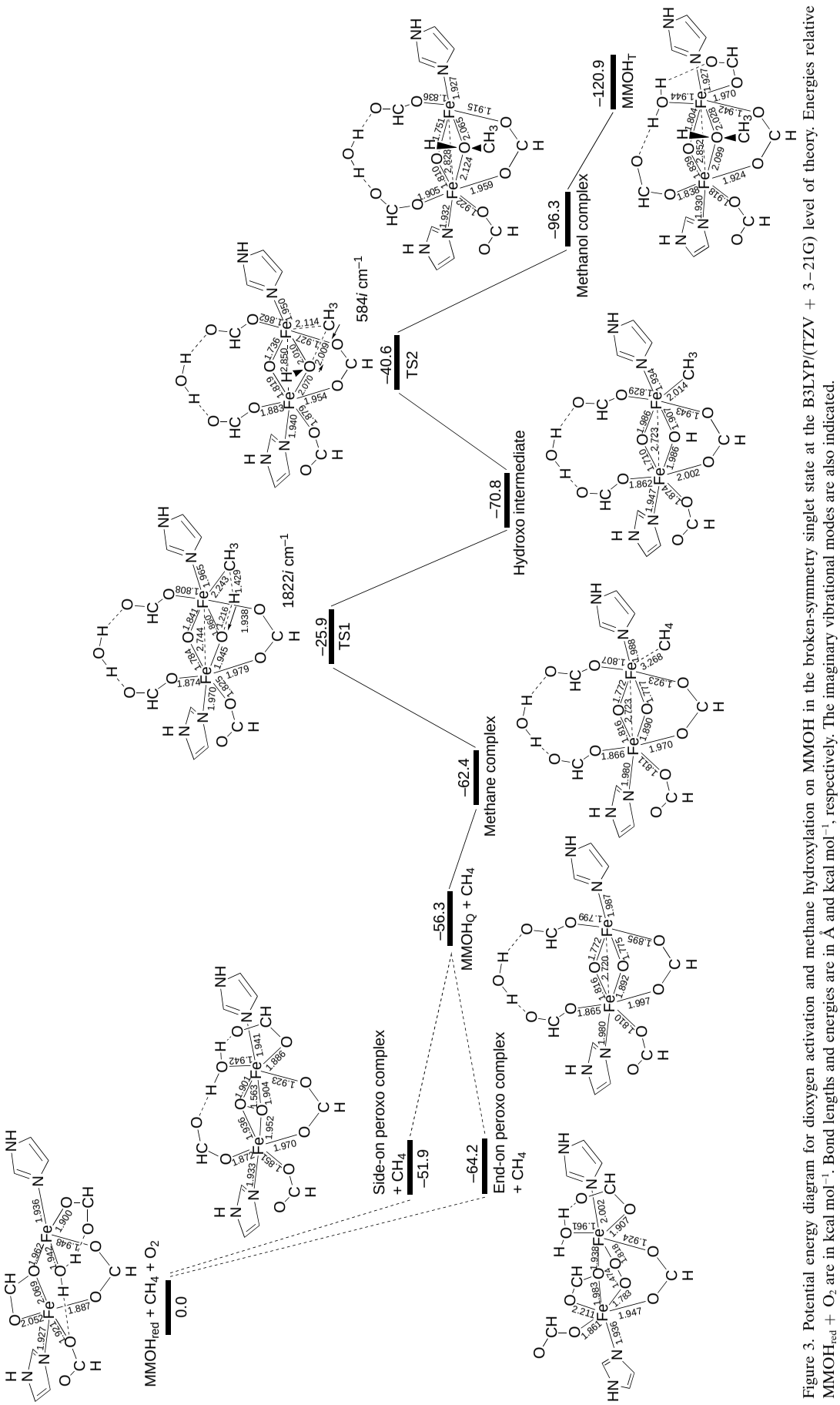

Figure 3. Potential energy diagram for dioxygen activation and methane hydroxylation on MMOH in the broken-symmetry singlet state at the B3LYP/(TZV + 3–21G) level of theory. Energies relative to MMOH$_{red}$ + O$_2$ are in kcal mol^{-1}. Bond lengths and energies are in Å and kcal mol^{-1}, respectively. The imaginary vibrational modes are also indicated.

bridging mode. In the end-on peroxo complex, the O–O distance is 1.474 Å, and the Fe–O distances are 1.783 and 1.818 Å. Earlier extended Hückel calculations demonstrated that this end-on bridging mode of peroxide is more favorable in energy than the side-on bridging mode.[45] Our B3LYP calculations also showed that the binding energy between dioxygen and the model of $MMOH_{red}$ in the end-on peroxo complex is 12.3 kcal mol^{-1} larger than that in the side-on peroxo complex. The two iron atoms and dioxygen do not lie in a plane in the side-on complex; the oxygen atoms are slightly distorted out of the line connecting the two iron atoms. The Fe–Fe distance is 3.307 Å and the O–O distance is 1.563 Å in the side-on model (Figure 3). After the activation of dioxygen, $MMOH_{peroxo}$ is converted into $MMOH_Q$, in which the bis(μ-oxo)diiron(IV) core is involved. B3LYP calculations tell us that the coordinatively unsaturated bis(μ-oxo)diiron(IV) model of $MMOH_Q$ lies 56.3 kcal mol^{-1} below the dissociation limit toward $MMOH_{red} + O_2$. Therefore, we propose from the energetic viewpoint that such a species can be formed in the catalytic cycle of MMOH and can be viewed as a reasonable model of $MMOH_Q$. From the viewpoint of known catalytic chemistry, as well as from that of perturbation theory,[46] it is in general reasonable to assume that catalytically active metal complexes might be coordinatively unsaturated. In the following discussion we describe a possible non-radical mechanism for the hydroxylation of methane taking place on this coordinatively unsaturated diiron model.

Reaction pathway for methane hydroxylation mediated by MMOH: Before looking at B3LYP results, let us consider the d orbital splitting of the coordinatively unsaturated diiron complex in order to gain a better understanding of its reactivity toward methane. We can derive useful information on essential differences between the saturated and unsaturated diiron complexes from orbital interaction analyses based on extended Hückel calculations.[45] As shown in Figure 4, the "t_{2g}" orbitals in the unsaturated diiron complex are partially occupied, as in those of the saturated diiron

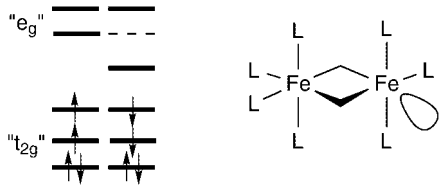

Figure 4. Production of a kind of nonbonding d orbital pointing toward the missing ligand in the coordinatively unsaturated diiron complex.

complex. In contrast to the saturated diiron complex, one of the unoccupied high-lying orbitals comes down into the frontier orbital region between the "t_{2g}" and "e_g" sets in the coordinatively unsaturated diiron complex. This orbital is a kind of nonbonding d orbital pointing toward the missing ligand and plays an important role in the binding of substrate methane. From the viewpoint of a simple second-order perturbation concept, interaction energy should be mainly governed by the energy separation of the interacting orbitals. Since the unoccupied nonbonding orbital lies below the "e_g" orbitals, the unsaturated diiron active center should exhibit high reactivity toward methane. The interaction between the unoccupied nonbonding orbital and the HOMO of methane plays an essential role in the dissociation of a C–H bond of methane.[46]

Let us next look at B3LYP computational results on the reaction pathway for methane hydroxylation on the coordinatively unsaturated bis(μ-oxo)diiron(IV) complex. Figure 3 shows a computed energy diagram for the conversion of methane into methanol and optimized geometries for the reaction species relevant to the hydroxylation reaction. The general profile of the diagram is downhill, so this hydroxylation reaction is expected to proceed spontaneously. We assumed here that methane should approach towards the active site of $MMOH_Q$ only from the side of the two formate ligands, because hydrophobic cavities at which methane binds favorably exist at a site distal to the two histidine residues.[47] An important stage in this non-radical mechanism is that the five-coordinate iron atom and substrate methane come into contact. In the resultant methane complex, the distance between the iron atom and the carbon atom of methane was calculated to be 3.268 Å; thus, it is a weakly bound encounter complex. After the formation of this complex, an H atom of methane is abstracted via a four-centered transition state (TS1). This process requires an activation energy of 30.4 kcal mol^{-1} relative to the dissociation limit toward $CH_4 + MMOH_Q$. It is interesting to consider whether or not the energy acquired by the reacting system in the dioxygen activation process can be used for the driving force of this reaction. Although, of course, the protein pocket partially absorbs this excess energy released in the dioxygen activation process, the transient intermediates can decay before complete equilibration of the system, and this energy is in part used to pass over the potential energy barrier for the H atom abstraction. The imaginary mode of vibration (1822 i cm^{-1}) with respect to TS1 shows that an H atom migrates from the bound methane to a bridging oxygen atom of the diiron model. Thus, the transition state for the intramolecular H atom migration leads to the formation of an important reaction intermediate that we call hydroxo intermediate.

TS1 in the non-radical mechanism is different in geometry from the transition state for the direct H atom abstraction (TS_{direct}) in the radical rebound mechanism.[14–16] The H atom abstraction from methane in TS1 takes place in a four-centered manner with a unique Fe–C bond, while that in TS_{direct} occurs in a linear C–H–O alignment. When one of the iron atoms in the diiron model has a vacant coordination site for methane, the Fe–C bond is reasonably formed in the course of methane activation. The C–H bond of methane is effectively activated through the orbital interaction discussed earlier.[17a, 46] On the other hand, there is no such vacant site in the coordinatively saturated diiron active center, and the iron atoms themselves cannot play a direct role in the cleavage of a C–H bond of methane. We optimized and obtained the transition state for direct H atom abstraction by the saturated diiron model in the nonet and undecet spin states (Figure 5). However, we could not locate the corresponding transition state on the singlet potential energy surface. To look at the energetics of the direct abstraction in the singlet state, we

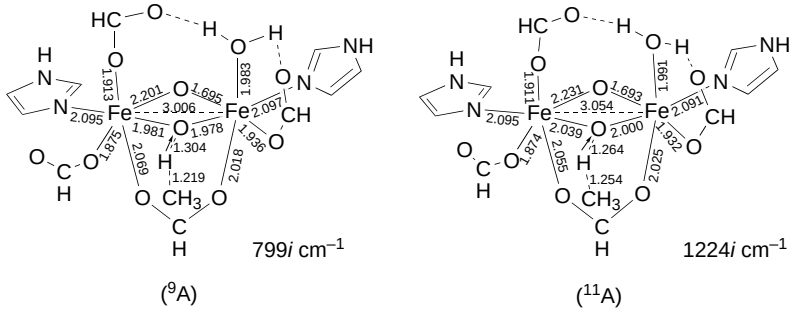

Figure 5. Optimized geometries of TS_{direct} in the nonet and undecet states. The imaginary vibrational modes are also given.

carried out a single-point calculation with the optimized structure of TS_{direct} (^{9}A). TS_{direct} (^{1}A) is 18.7 and 16.7 kcal mol^{-1} less stable than TS_{direct} (^{9}A) and TS_{direct} (^{11}A), respectively. According to the B3LYP calculations, the imaginary modes of vibration (799i cm^{-1} (^{9}A) and 1224i cm^{-1} (^{11}A)) in TS_{direct} show that one of the H atoms of methane migrates toward a bridging oxygen atom. The bridging oxygen atoms in these high-spin states have significant spin densities, whereas those in the broken-symmetry singlet state do not have spin densities large enough to activate methane. This difference results in the different mechanisms with respect to the H atom abstraction.

The geometrical features of the four-centered structure of TS1 in sMMO are similar to those of the transition state for the H atom abstraction from methane by the bare FeO^+ complex with respect to the lengths of the C–H bond being dissociated and the O–H bond being formed, as well as the bond angles, as shown in Figure 6. In the H atom abstraction

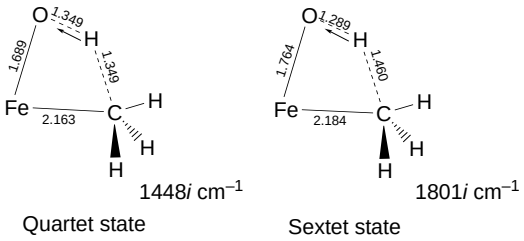

Figure 6. Optimized geometries of the transition states for H atom abstraction from methane by FeO^+ in the quartet and in the sextet states at the B3LYP/TZV level of theory. Bond lengths are in Å. The imaginary vibrational modes are also given.

by FeO^+, the 3σ orbital of FeO^+ indicated on the left-hand side of Figure 7 plays an important role in the C–H bond activation of methane.[19c] In the $MMOH_Q$ active site model, the relevant nonbonding orbital shown on the right hand side of Figure 7 should be responsible for the interaction between methane and $MMOH_Q$. The nonbonding orbital in the right-hand iron-oxo unit of $MMOH_Q$ has an orbital feature similar to the 3σ orbital of FeO^+, and it is therefore reasonable that the C–H bond activation of methane occurs in a fashion similar to the FeO^+ case. In the reaction between methane and FeO^+, only the four-centered hydrogen-atom abstraction occurs in the low-spin quartet state, whereas both four-centered and direct hydrogen-atom abstractions occur in the high-spin sextet state.[19c] The nonbonding orbitals indicated in Figure 7 are singly occupied in the high-spin states, and these orbitals therefore play a role as a radical carrier. On the other hand, they are unoccupied in the low-spin states and play an important role as an "acceptor orbital". This striking difference leads us to consider the different hydroxylation mechanisms in a high-spin state and in a low-spin state.

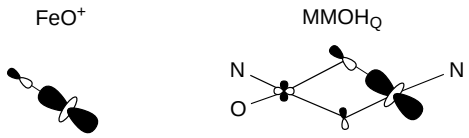

Figure 7. Role played by the 3σ orbital of FeO^+ in H atom abstraction by FeO^+ (left) and the relevant nonbonding orbital responsible for the interaction between methane and $MMOH_Q$ in the $MMOH_Q$ active site model (right).

After the hydrogen-atom abstraction via TS1, a hydroxo intermediate is formed, in which newly formed OH and CH_3 groups directly coordinate to an iron atom as ligands. This intermediate corresponds to the important insertion species ($HO\text{-}Fe^+\text{-}CH_3$) in the methane–methanol conversion by FeO^+ in the gas phase.[19] A computed spin density on the methyl group is 0.3, which is of course small relative to that of the methyl group in the radical intermediate ($\approx$1.0).[15a] After the formation of the hydroxo intermediate, the hydrogen atom of the OH group rotates out of the $Fe_2(\mu\text{-}O)_2$ plane and the methyl group migrates toward the OH group via the three-centered transition state in the second step (TS2). This corresponds to the rebound step in P450-mediated hydroxylation.[9] In this transition state, the Fe–C bond is cleaved and instead the C–O bond is newly formed. The barrier height of TS2 is 15.7 kcal mol^{-1} relative to the dissociation limit toward $CH_4 + MMOH_Q$. A methanol complex is formed after TS2, through the binding of the methyl and hydroxo ligands. In this complex, newly formed methanol is involved as a ligand; the oxygen atom of the methanol moiety is bound to the two iron atoms. In the very final stages of the reaction, the released water returns to the five-coordinate iron atom, resulting in another methanol complex, the iron atoms of which are coordinatively saturated. This final complex, in which methanol occupies a bridging position between the two iron atoms, corresponds to intermediate T ($MMOH_T$).[7a] The computed lengths of the Fe–O bonds are 2.099 and 2.028 Å, in good agreement with those of the X-ray structure of methanol-containing $MMOH_{ox}$.[48] The final complex is 120.9 kcal mol^{-1} more stable than the dissociation limit toward $CH_4 + O_2 + MMOH_{red}$. The excess energy can be partly used for the release of the methanol ligand and can be released into protein surroundings in the course of the reaction.

Finally we discuss the observed inversion of stereochemistry at a labeled carbon for sMMO-catalyzed hydroxylation.

Floss and co-workers reported that chiral ethane hydroxylation occurs predominantly (64–74%) with retention of configuration in both the Bath and the OB3b systems.[10, 13] According to a recent semiclassical molecular dynamics simulation, a mixture of a radical and a non-synchronous concerted mechanism can explain the experimental results.[16d] Our non-radical mechanism, of course, conserves stereochemistry in the course of the reaction, but we have suggested that the inversion of methane itself can occur via a C_s transition state on transition metal complexes.[49] The transformation of tetrahedral to planar methane through a symmetry-allowed process for either a twisting or a squashing pathway has been a central issue in theoretical chemistry,[50] and we have suggested that methane inversion can occur when it forms an adduct with a transition metal complex. Since a carbon atom that loosely coordinates to a metal active center can undergo pseudorotation, the inversion of methane can occur at a coordinatively unsaturated active center of an enzyme. Thus, our non-radical mechanism can also explain the observed loss of stereochemistry in hydroxylations by sMMO.

Kinetic isotope effects for hydrogen-atom abstraction from methane: Figure 3 shows that the activation energy for H atom abstraction via TS1 is higher than that for the rebound step via TS2; the rate-determining step in the course of methane hydroxylation on $MMOH_Q$ should therefore be the activation of a C–H bond of methane. In this section we consider kinetic isotope effects for H atom abstraction at the active site of $MMOH_Q$. From the decay of $MMOH_Q$, Lipscomb and co-workers measured KIEs for the C–H bond activation of methane on MMOH and reported surprisingly large KIEs, falling in the 50–100 range.[20] Analysis of product distribution after a single turnover gave KIEs of 4–19 at 277 K; for example, 19 ± 3.9 for 1:1 CH_4:CD_4, 12 ± 1 for CD_3H, 9 ± 0.5 for CD_2H_2, and 3.9 ± 1 for CDH_3.[20] According to the KIE analyses, secondary kinetic isotope effects appear to have little or no effect on the KIEs from the decay of $MMOH_Q$, but much more significant effects on the KIEs from the analysis of product distributions. Lippard and co-workers also reported a smaller, but still large, KIE of 28 from the decay of $MMOH_Q$.[6e] These large KIEs are expected to originate from hydrogen tunneling during the H atom abstraction.

We calculated the KIE for H atom abstraction via TS1 and TS_{direct} by transition state theory, which leads to the expression (2), where subscripts H and D stand for the hydrogen and deuterium-substituted forms, respectively, superscripts R and # represent the reactant methane and the transition state, respectively, q_v stands for the vibrational partition function, I is the principal moments of inertia, m is molecular mass, and $E^{\#}$ is the activation energy measured from the reactant complex on each potential energy surface and includes zero-point vibrational energies (ZPVEs).

$$\frac{k_H}{k_D} = \left(\frac{m_D^R m_H^{\#}}{m_H^R m_D^{\#}}\right)^{3/2} \left(\frac{I_{xD}^R I_{yD}^R I_{zD}^R}{I_{xH}^R I_{yH}^R I_{zH}^R}\right)^{1/2} \left(\frac{I_{xH}^{\#} I_{yH}^{\#} I_{zH}^{\#}}{I_{xD}^{\#} I_{yD}^{\#} I_{zD}^{\#}}\right)^{1/2} \times \frac{q_{vD}^R q_{vH}^{\#}}{q_{vH}^R q_{vD}^{\#}} \exp\left(-\frac{E_H^{\#} - E_D^{\#}}{RT}\right) \quad (2)$$

We adopted CD_4, CD_3H, CD_2H_2, and CDH_3 as deuterium-substituted forms of methane. In addition, we added Wigner tunneling corrections to data obtained from transition state theory.[51] The tunneling correction coefficient is written in the form of $\kappa = 1 - 1/24(h\nu^{\ddagger}/kT)^2$, where $\nu^{\ddagger}$ is the imaginary frequency with respect to the transition state for the hydrogen abstraction. As a consequence, the KIEs with Wigner tunneling corrections can be calculated from the expression of $\kappa_H k_H / \kappa_D k_D$.

Table 2 lists computed KIEs for H atom abstraction via TS1. The values in parentheses include Wigner's tunneling corrections. As would be expected from the form of Equation (2), the KIEs decrease significantly as temperature increases. At 277 K the KIE for H/D atom abstraction from CH_4/CD_2H_2 was computed as 6.3 (9.7) on the basis of transition state theory (with Wigner tunneling corrections).

Table 2. Computed k_H/k_D values for H atom abstraction from methane by $MMOH_Q$ via the four-centered transition state (TS1) in the broken-symmetry singlet state. The values in parentheses include Wigner's tunneling corrections.

T [K]	CD_4	CD_3H	CD_2H_2	CDH_3
200	14.8 (25.2)	11.8 (19.7)	9.7 (16.1)	8.3 (13.6)
250	10.8 (17.7)	8.7 (13.9)	7.1 (11.3)	6.0 (9.4)
277	9.5 (15.1)	6.9 (10.7)	6.3 (9.7)	5.3 (8.1)
300	8.6 (13.3)	5.8 (8.5)	5.7 (8.7)	4.8 (7.2)
350	7.1 (10.5)	5.0 (7.1)	4.8 (7.1)	4.1 (5.9)

The value is about 1.5 times larger when we take the tunneling effect into account. The KIE including tunneling corrections is in good agreement with the value obtained by analysis of product distributions (9.3 ± 0.5, 277 K). The KIEs decrease as the number of deuterium atoms involved in substrate methane decreases, because the vibrational frequencies significantly decrease when the number of deuterium atoms involved is large. The computed KIEs for H/D abstraction from methane agree with the experimental KIEs, except for CH_4/CDH_3.

Table 3 presents computed KIEs for direct hydrogen-atom abstraction via TS_{direct}. At 277 K a computed value for direct H(D) atom abstraction from CH_4 (CD_2H_2) in the nonet state is 8.3 in transition state theory, and this quantity increases to 9.9 with tunneling corrections. At 277 K the value for direct hydrogen-atom abstraction without tunneling corrections is large in comparison with that for the four-centered H atom abstraction. However, if we take a tunneling effect into account, the values in TS1 and in TS_{direct} with respect to the H atom abstraction are essentially similar and not distinguish-

Table 3. Computed k_H/k_D values for H atom abstraction from methane by $MMOH_Q$ via the linear transition state (TS_{direct}) in the high-spin nonet state. The values in parentheses include Wigner's tunneling corrections.

T [K]	CD_4	CD_3H	CD_2H_2	CDH_3
200	22.3 (29.5)	17.9 (23.4)	15.0 (19.5)	11.9 (15.1)
250	14.1 (17.7)	11.6 (14.4)	9.8 (12.1)	7.9 (9.5)
277	11.8 (14.3)	9.8 (11.8)	8.3 (9.9)	6.7 (7.9)
300	10.2 (12.2)	8.6 (10.1)	7.3 (8.6)	6.0 (6.9)
350	7.9 (9.1)	6.8 (7.7)	4.8 (7.0)	4.1 (4.6)

able. This is a direct consequence arising from the framework of Wigner's tunneling correction, and so the change in the imaginary frequency should be responsible for the determination of KIEs. When we replace CH_4 with CD_2H_2, the imaginary frequency in TS1 changes from $1822\,i\,cm^{-1}$ to $1351\,i\,cm^{-1}$, while that in TS_{direct} changes from $799\,i\,cm^{-1}$ to $620\,i\,cm^{-1}$. The change in TS1 is larger than that in TS_{direct}, and the tunneling effect therefore has a greater effect on TS1.

Conclusion

By use of quantum-chemical calculations at the B3LYP DFT level, we have considered a non-radical mechanism for methane hydroxylation, using a coordinatively unsaturated bis(μ-oxo)diiron(IV) complex as a model of the active site of $MMOH_Q$. A water ligand is released from one of the iron atoms in the coordinatively saturated diiron complex, to become weakly bound to two formate ligands through hydrogen bonds. Thus, one iron atom in our model of the active site of $MMOH_Q$ is five-coordinate while the other remains six-coordinate. From the viewpoint of energy in DFT computations, we found that such a species is generated in the course of the catalytic reaction. Since this model has a vacant coordination site for substrate methane, methane hydroxylation can take place in the singlet state in a manner different from the widely believed radical rebound mechanism. In the non-radical mechanism that we propose, a C–H bond of methane is dissociated via a four-centered transition state (TS1) in which an interesting Fe–C bond is involved. The four-centered H atom abstraction from methane leads to a hydroxo intermediate in which the newly formed OH and CH_3 groups directly coordinate to one of the iron atoms. In the second step of the reaction, the methyl ligand and the OH ligand are bound via a three-centered transition state (TS2), resulting in the formation of a methanol complex. In the very final stages of the reaction, the released water comes back to the five-coordinate iron atom, resulting in another methanol complex, the iron atoms of which are coordinatively saturated. This mechanism is essentially identical to that of methane–methanol conversion by the bare FeO^+ complex and relevant transition metal–oxo complexes in the gas phase. Neither radical species nor ionic species are involved in this mechanism. We also analyzed kinetic isotope effects (KIEs) in the H atom abstraction from methane, which is the rate-determining step in this hydroxylation reaction. Computed KIEs in the four-centered abstraction and the direct abstraction are essentially similar and are not distinguishable.

Acknowledgements

K.Y. acknowledges the Ministry of Culture, Sports, Science, and Technology of Japan, the Japan Society for the Promotion of Science, the Iwatani Naoji Foundation, the Takeda Science Foundation, and Kyushu University P & P "Green Chemistry" for their support of this work. T.Y. thanks the Japan Society for the Promotion of Science for a graduate fellowship. Computations were in part carried out at the Computer Center of the Institute for Molecular Science.

[1] Recent reviews on MMO: a) A. L. Feig, S. J. Lippard, *Chem. Rev.* **1994**, *94*, 759; b) J. D. Lipscomb, *Annu. Rev. Microbiol.* **1994**, *48*, 371; c) K. E. Liu, S. J. Lippard, *Adv. Inorg. Chem.* **1995**, *42*, 263; d) B. J. Wallar, J. D. Lipscomb, *Chem. Rev.* **1996**, *96*, 2625; e) L. Que Jr., Y. Dong, *Acc. Chem. Res.* **1996**, *29*, 190; f) A. M. Valentine, S. J. Lippard, *J. Chem. Soc. Dalton Trans.* **1997**, 3925; g) D. M. Kurtz Jr., *J. Biol. Inorg. Chem.* **1997**, *2*, 159; h) M. Merkx, D. A. Kopp, M. H. Sazinsky, J. L. Blazyk, J. Müller, S. J. Lippard, *Angew. Chem.* **2001**, *113*, 2860; *Angew. Chem. Int. Ed.* **2001**, *40*, 2782.

[2] a) J. Colby, H. Dalton, *Biochem. J.* **1978**, *171*, 461; b) M. P. Woodland, H. Dalton, *J. Biol. Chem.* **1984**, *259*, 53; c) B. G. Fox, W. A. Froland, J. E. Dege, J. D. Lipscomb, *J. Biol. Chem.* **1989**, *264*, 10023; d) G. T. Gassner, S. J. Lippard, *Biochemistry* **1999**, *38*, 12768.

[3] a) M. P. Woodland, D. S. Patil, R. Cammack, H. Dalton, *Biochim. Biophys. Acta* **1986**, *873*, 237; b) A. Ericson, B. Hedman, K. O. Hodgson, J. Green, H. Dalton, J. G. Bentsen, R. H. Beer, S. J. Lippard, *J. Am. Chem. Soc.* **1988**, *110*, 2330; c) B. G. Fox, K. K. Surerus, E. Münck, J. D. Lipscomb, *J. Biol. Chem.* **1988**, *263*, 10553; d) A. C. Rosenzweig, C. A. Frederick, S. J. Lippard, P. Nordlund, *Nature* **1993**, *366*, 537; e) A. C. Rosenzweig, P. Nordlund, P. M. Takahara, C. A. Frederick, S. J. Lippard, *Chem. Biol.* **1995**, *2*, 409; f) D. A. Whittington, S. J. Lippard, *J. Am. Chem. Soc.* **2001**, *123*, 827.

[4] a) B. G. Fox, Y. Liu, J. E. Dege, J. D. Lipscomb, *J. Biol. Chem.* **1991**, *266*, 540; b) W. A. Froland, K. K. Andersson, S.-K. Lee, Y. Liu, J. D. Lipscomb, *J. Biol. Chem.* **1992**, *267*, 17588; c) K. E. Paulsen, Y. Liu, B. G. Fox, J. D. Lipscomb, E. Münck, M. T. Stankovich, *Biochemistry* **1994**, *33*, 713; d) Y. Liu, J. C. Nesheim, S.-K. Lee, J. D. Lipscomb, *J. Biol. Chem.* **1995**, *270*, 24662; e) S. C. Pulver, W. A. Froland, J. D. Lipscomb, E. I. Solomon, *J. Am. Chem. Soc.* **1997**, *119*, 387; f) Y. Liu, J. C. Nesheim, K. E. Paulsen, M. T. Stankovich, J. D. Lipscomb, *Biochemistry* **1997**, *36*, 5223; g) B. J. Wallar, J. D. Lipscomb, *Biochemistry* **2001**, *40*, 2220; h) B. J. Brazeau, B. J. Wallar, J. D. Lipscomb, *J. Am. Chem. Soc.* **2001**, *123*, 10421.

[5] a) J. Lund, H. Dalton, *Eur. J. Biochem.* **1985**, *147*, 291; b) J. Lund, M. P. Woodland, H. Dalton, *Eur. J. Biochem.* **1985**, *147*, 297.

[6] a) K. E. Liu, D. Wang, B. H. Huynh, D. E. Edmondson, A. Salifoglou, S. J. Lippard, *J. Am. Chem. Soc.* **1994**, *116*, 7465; b) K. E. Liu, A. M. Valentine, D. Qiu, D. E. Edmondson, E. H. Appelman, T. G. Spiro, S. J. Lippard, *J. Am. Chem. Soc.* **1995**, *117*, 4997; c) K. E. Liu, A. M. Valentine, D. Wang, B. H. Huynh, D. E. Edmondson, A. Salifoglou, S. J. Lippard, *J. Am. Chem. Soc.* **1995**, *117*, 10174; d) S.-K. Lee, J. D. Lipscomb, *Biochemistry* **1999**, *38*, 4423; e) A. M. Valentine, S. S. Stahl, S. J. Lippard, *J. Am. Chem. Soc.* **1999**, *121*, 3876; f) B. J. Brazeau, J. D. Lipscomb, *Biochemistry* **2000**, *39*, 13503.

[7] a) S.-K. Lee, J. C. Nesheim, J. D. Lipscomb, *J. Biol. Chem.* **1993**, *268*, 21569; b) S.-K. Lee, B. G. Fox, W. A. Froland, J. D. Lipscomb, E. Münck, *J. Am. Chem. Soc.* **1993**, *115*, 6450.

[8] L. Shu, J. C. Nesheim, K. Kauffmann, E. Münck, J. D. Lipscomb, L. Que Jr., *Science* **1997**, *275*, 515.

[9] a) *Cytochrome P450*: *Structure*, *Mechanism*, *and Biochemistry*, 2nd ed. (Ed.: P. R. Ortiz de Montellano), Plenum, New York, **1995**; b) M. Sono, M. P. Roach, E. D. Coulter, J. H. Dawson, *Chem. Rev.* **1996**, *96*, 2841.

[10] N. D. Priestley, H. G. Floss, W. A. Froland, J. D. Lipscomb, P. G. Williams, H. Morimoto, *J. Am. Chem. Soc.* **1992**, *114*, 7561.

[11] a) K. E. Liu, C. C. Johnson, M. Newcomb, S. J. Lippard, *J. Am. Chem. Soc.* **1993**, *115*, 939; b) S.-Y. Choi, P. E. Eaton, P. F. Hollenberg, K. E. Liu, S. J. Lippard, M. Newcomb, D. A. Putt, S. P. Upadhyaya, Y. Xiong, *J. Am. Chem. Soc.* **1996**, *118*, 6547; c) A. M. Valentine, M. H. LeTadic-Biadatti, P. H. Toy, M. Newcomb, S. J. Lippard, *J. Biol. Chem.* **1999**, *274*, 10771; d) S.-Y. Choi, P. E. Eaton, D. A. Kopp, S. J. Lippard, M. Newcomb, R. Shen, *J. Am. Chem. Soc.* **1999**, *121*, 12198.

[12] a) Y. Jin, J. D. Lipscomb, *Biochemistry* **1999**, *38*, 6178; b) B. J. Brazeau, R. N. Austin, C. Tarr, J. T. Groves, J. D. Lipscomb, *J. Am. Chem. Soc.* **2001**, *123*, 11831.

[13] A. M. Valentine, B. Wilkinson, K. E. Liu, S. Komar-Panicucci, N. D. Priestley, P. G. Williams, H. Morimoto, H. G. Floss, S. J. Lippard, *J. Am. Chem. Soc.* **1997**, *119*, 1818.

[14] a) P. E. M. Siegbahn, R. H. Crabtree, *J. Am. Chem. Soc.* **1997**, *119*, 3103; b) P. E. M. Siegbahn, R. H. Crabtree, P. Nordlund, *J. Biol. Inorg. Chem.* **1998**, *3*, 314; c) P. E. M. Siegbahn, *Inorg. Chem.* **1999**, *38*, 2880; d) P. E. M. Siegbahn, M. R. A. Blomberg, *Chem. Rev.* **2000**, *100*, 421;

e) P. E. M. Siegbahn, *J. Biol. Inorg. Chem.* **2001**, *6*, 27; f) P. E. M. Siegbahn, *Chem. Phys. Lett.* **2002**, *351*, 311.

[15] a) H. Basch, K. Mogi, D. G. Musaev, K. Morokuma, *J. Am. Chem. Soc.* **1999**, *121*, 7249; b) M. Torrent, D. G. Musaev, K. Morokuma, *J. Phys. Chem. B* **2001**, *105*, 322; c) H. Basch, D. G. Musaev, K. Mogi, K. Morokuma, *J. Phys. Chem. A* **2001**, *105*, 3615; d) M. Torrent, D. G. Musaev, H. Basch, K. Morokuma, *J. Phys. Chem. B* **2001**, *105*, 4453; e) M. Torrent, K. Mogi, H. Basch, D. G. Musaev, K. Morokuma, *J. Phys. Chem. B* **2001**, *105*, 8616; f) H. Basch, D. G. Musaev, K. Morokuma, *J. Phys. Chem. B* **2001**, *105*, 8452; g) M. Torrent, D. G. Musaev, H. Basch, K. Morokuma, *J. Comput. Chem.* **2002**, *23*, 59; h) M. Torrent, T. Vreven, D. G. Musaev, K. Morokuma, O. Farkas, H. B. Schlegel, *J. Am. Chem. Soc.* **2002**, *124*, 192.

[16] a) B. D. Dunietz, M. D. Beachy, Y. Cao, D. A. Whittington, S. J. Lippard, R. A. Friesner, *J. Am. Chem. Soc.* **2000**, *122*, 2828; b) B. F. Gherman, B. D. Dunietz, D. A. Whittington, S. J. Lippard, R. A. Friesner, *J. Am. Chem. Soc.* **2001**, *123*, 3836; c) R. A. Friesner, B. D. Dunietz, *Acc. Chem. Res.* **2001**, *34*, 351; d) V. Guallar, B. F. Gherman, W. H. Miller, S. J. Lippard, R. A. Friesner, *J. Am. Chem. Soc.* **2002**, *124*, 3377.

[17] a) K. Yoshizawa, T. Ohta, T. Yamabe, R. Hoffmann, *J. Am. Chem. Soc.* **1997**, *119*, 12311; b) K. Yoshizawa, *J. Biol. Inorg. Chem.* **1998**, *3*, 318; c) K. Yoshizawa, T. Ohta, T. Yamabe, *Bull. Chem. Soc. Jpn.* **1998**, *71*, 1899; d) K. Yoshizawa, A. Suzuki, Y. Shiota, T. Yamabe, *Bull. Chem. Soc. Jpn.* **2000**, *73*, 815; e) K. Yoshizawa, *J. Inorg. Biochem.* **2000**, *78*, 23.

[18] a) D. Schröder, H. Schwarz, *Angew. Chem.* **1995**, *107*, 2126; *Angew. Chem. Int. Ed. Engl.* **1995**, *34*, 1973; b) D. Schröder, H. Schwarz, *Angew. Chem.* **1990**, *102*, 1468; *Angew. Chem. Int. Ed. Engl.* **1990**, *29*, 1433; c) D. Schröder, A. Fiedler, J. Hrusák, H. Schwarz, *J. Am. Chem. Soc.* **1992**, *114*, 1215; d) D. Schröder, H. Schwarz, D. E. Clemmer, Y.-M. Chen, P. B. Armentrout, V. I. Baranov, D. K. Böhme, *Int. J. Mass Spectrom. Ion Processes* **1997**, *161*, 175; e) D. Schröder, H. Schwarz, *Helv. Chim. Acta* **1992**, *75*, 1281; f) H. Becker, D. Schröder, W. Zummack, H. Schwarz, *J. Am. Chem. Soc.* **1994**, *116*, 1096; g) M. F. Ryan, D. Stöckigt, H. Schwarz, *J. Am. Chem. Soc.* **1994**, *116*, 9565; h) S. Shaik, D. Danovich, A. Fiedler, D. Schröder, H. Schwarz, *Helv. Chim. Acta* **1995**, *78*, 1393; i) A. Fiedler, D. Schröder, S. Shaik, H. Schwarz, *J. Am. Chem. Soc.* **1994**, *116*, 10734.

[19] a) K. Yoshizawa, Y. Shiota, T. Yamabe, *Chem. Eur. J.* **1997**, *3*, 1160; b) K. Yoshizawa, Y. Shiota, T. Yamabe, *J. Am. Chem. Soc.* **1998**, *120*, 564; c) K. Yoshizawa, Y. Shiota, T. Yamabe, *Organometallics* **1998**, *17*, 2825; d) Y. Shiota, K. Yoshizawa, *J. Am. Chem. Soc.* **2000**, *122*, 12317.

[20] J. C. Nesheim, J. D. Lipscomb, *Biochemistry* **1996**, *35*, 10240.

[21] a) L. Noodleman, *J. Chem. Phys.* **1981**, *74*, 5737; b) L. Noodleman, E. R. Davidson, *Chem. Phys.* **1986**, *109*, 131; c) L. Noodleman, C. Y. Peng, D. A. Case, J. M. Mouesca, *Coord. Chem. Rev.* **1995**, *144*, 199.

[22] a) A. Bencini, D. Gatteschi, *J. Am. Chem. Soc.* **1986**, *108*, 5763; b) C. Albonico, A. Bencini, *Inorg. Chem.* **1988**, *27*, 1934; c) A. Bencini, *J. Chim. Phys.* **1989**, *86*, 763; d) A. Bencini, F. Totti, C. A. Daul, K. Doclo, P. Fantucci, V. Barone, *Inorg. Chem.* **1997**, *36*, 5022; e) V. Barone, A. Bencini, I. Ciofini, C. A. Daul, F. Totti, *J. Am. Chem. Soc.* **1998**, *120*, 8357; f) V. Barone, A. Bencini, M. Cossi, A. Di Matteo, M. Mattesini, F. Totti, *J. Am. Chem. Soc.* **1998**, *120*, 7069; g) A. Bencini, D. Gatteschi, F. Totti, D. N. Sanz, J. A. McCleverty, M. D. Ward, *J. Phys. Chem. A* **1998**, *102*, 10545; h) C. Adamo, V. Barone, A. Bencini, F. Totti, I. Ciofini, *Inorg. Chem.* **1999**, *38*, 1996.

[23] a) P. K. Ross, E. I. Solomon, *J. Am. Chem. Soc.* **1991**, *113*, 3246; b) T. C. Brunold, N. Tamura, N. Kitajima, Y. Moro-Oka, E. I. Solomon, *J. Am. Chem. Soc.* **1998**, *120*, 5674; c) T. C. Brunold, E. I. Solomon, *J. Am. Chem. Soc.* **1999**, *121*, 8277; d) T. C. Brunold, E. I. Solomon, *J. Am. Chem. Soc.* **1999**, *121*, 8288.

[24] a) R. Stranger, P. W. Smith, I. E. Grey, *Inorg. Chem.* **1989**, *28*, 1271; b) G. A. Medley, R. Stranger, *Inorg. Chem.* **1994**, *33*, 3976; c) T. Lovell, J. E. McGrady, R. Stranger, S. A. Macgregor, *Inorg. Chem.* **1996**, *35*, 3079; d) J. E. McGrady, R. Stranger, *J. Am. Chem. Soc.* **1997**, *119*, 8512; e) J. E. McGrady, T. Lovell, R. Stranger, *Inorg. Chem.* **1997**, *36*, 3242; f) J. E. McGrady, R. Stranger, T. Lovell, *J. Phys. Chem. A* **1997**, *101*, 6265; g) J. E. McGrady, R. Stranger, T. Lovell, *Inorg. Chem.* **1998**, *37*, 3802; h) J. E. McGrady, *Angew. Chem.* **2000**, *112*, 3216; *Angew. Chem. Int. Ed.* **2000**, *17*, 3077; i) C. D. Delfs, R. Stranger, *Inorg. Chem.* **2001**, *40*, 3061.

[25] a) E. Ruiz, P. Alemany, S. Alvarez, J. Cano, *J. Am. Chem. Soc.* **1997**, *119*, 1297; b) E. Ruiz, P. Alemany, S. Alvarez, J. Cano, *Inorg. Chem.* **1997**, *36*, 3683; c) E. Ruiz, S. Alvarez, P. Alemany, *Chem. Commun.* **1998**, 2762; d) E. Ruiz, J. Cano, S. Alvarez, P. Alemany, *J. Am. Chem. Soc.* **1998**, *120*, 11122; e) J. Cano, P. Alemany, S. Alvarez, M. Verdaguer, E. Ruiz, *Chem. Eur. J.* **1998**, *4*, 476; f) J. Cano, E. Ruiz, P. Alemany, F. Lloret, S. Alvarez, *J. Chem. Soc. Dalton Trans.* **1999**, 1669; g) E. Ruiz, J. Cano, S. Alvarez, P. Alemany, *J. Comput. Chem.* **1999**, *20*, 1391; h) J. Cano, A. Rodriguez-Fortea, P. Alemany, S. Alvarez, E. Ruiz, *Chem. Eur. J.* **2000**, *6*, 327; i) F. F. Biani, E. Ruiz, J. Cano, J. J. Novoa, S. Alvarez, *Inorg. Chem.* **2000**, *39*, 3221.

[26] a) L. Noodleman, D. A. Case, *Adv. Inorg. Chem.* **1992**, *38*, 423; b) J. M. Mouesca, J. L. Chen, L. Noodleman, D. Bashford, D. A. Case, *J. Am. Chem. Soc.* **1994**, *116*, 11898; c) J. L. Chen, L. Noodleman, D. A. Case, D. Bashford, *J. Phys. Chem. A* **1994**, *98*, 11059; d) X. G. Zhao, W. H. Richardson, J. L. Chen, L. Noodleman, H. L. Tsai, D. N. Hendrickson, *Inorg. Chem.* **1997**, *36*, 1198; e) J. Li, M. R. Nelson, C. Y. Peng, D. Bashford, L. Noodleman, *J. Phys. Chem. A* **1998**, *102*, 6311; f) T. Lovell, J. Li, L. Noodleman, *Inorg. Chem.* **2001**, *40*, 5251; g) T. Lovell, J. Li, L. Noodleman, *Inorg. Chem.* **2001**, *40*, 5267; h) T. Lovell, J. Li, T. Liu, D. A. Case, L. Noodleman, *J. Am. Chem. Soc.* **2001**, *123*, 12392; i) T. Lovell, W.-G. Han, T. Liu, L. Noodleman, *J. Am. Chem. Soc.* **2002**, *124*, 5890; j) T. Lovell, J. Li, D. A. Case, L. Noodleman, *J. Am. Chem. Soc.* **2002**, *124*, 4546.

[27] a) R. Caballol, O. Castell, F. Illas, I. de P. R. Moreira, J. P. Malrieu, *J. Phys. Chem. A* **1997**, *101*, 7860; b) F. Illas, R. L. Martin, *J. Chem. Phys.* **1998**, *108*, 2519.

[28] a) J. R. Hart, A. K. Rappé, S. M. Gorun, T. H. Upton, *Inorg. Chem.* **1992**, *31*, 5254; b) J. R. Hart, A. K. Rappé, S. M. Gorun, T. H. Upton, *J. Phys. Chem.* **1992**, *96*, 6264.

[29] F. Yan, Z. Chen, *J. Phys. Chem. A* **2000**, *104*, 6295.

[30] K. Yamaguchi, T. Fueno, N. Ueyama, A. Nakamura, M. Ozaki, *Chem. Phys. Lett.* **1989**, *164*, 210.

[31] B. Delley, A. J. Freeman, D. E. Ellis, *Phys. Rev. Lett.* **1983**, *50*, 488.

[32] a) A. D. Becke, *Phys. Rev. A* **1988**, *38*, 3098; b) A. D. Becke, *J. Chem. Phys.* **1993**, *98*, 5648; c) P. J. Stephens, F. J. Devlin, C. F. Chabalowski, M. J. Frisch, *J. Phys. Chem.* **1994**, *98*, 11623.

[33] C. Lee, W. Yang, R. G. Parr, *Phys. Rev. B* **1988**, *37*, 785.

[34] M. J. Frisch, G. W. Trucks, H. B. Schlegel, G. E. Scuseria, M. A. Robb, J. R. Cheeseman, V. G. Zakrzewski, J. A. Montgomery, R. E. Stratmann, J. C. Burant, S. Dapprich, J. M. Millam, A. D. Daniels, K. N. Kudin, M. C. Strain, O. Farkas, J. Tomasi, V. Barone, M. Cossi, R. Cammi, B. Mennucci, C. Pomelli, C. Adamo, S. Clifford, J. Ochterski, G. A. Petersson, P. Y. Ayala, Q. Cui, K. Morokuma, D. K. Malick, A. D. Rabuck, K. Raghavachari, J. B. Foresman, J. Cioslowski, J. V. Ortiz, B. B. Stefanov, G. Liu, A. Liashenko, P. Piskorz, I. Komaromi, R. Gomperts, R. L. Martin, D. J. Fox, T. Keith, M. A. Al-Laham, C. Y. Peng, A. Nanayakkara, C. Gonzalez, M. Challacombe, P. M. W. Gill, B. G. Johnson, W. Chen, M. W. Wong, J. L. Andres, M. Head-Gordon, E. S. Replogle, J. A. Pople, *Gaussian 98*, Gaussian Inc., Pittsburgh, PA, **1998**.

[35] S. H. Vosko, L. Wilk, M. Nusair, *Can. J. Phys.* **1980**, *58*, 1200.

[36] A. Schäfer, C. Huber, R. Ahlrichs, *J. Chem. Phys.* **1994**, *100*, 5829.

[37] J. S. Binkley, J. A. Pople, W. Hehre, *J. Am. Chem. Soc.* **1980**, *102*, 939.

[38] M. S. Gordon, J. S. Binkley, J. A. Pople, W. J. Pietro, W. J. Hehre, *J. Am. Chem. Soc.* **1982**, *104*, 2797.

[39] K. D. Dobbs, W. J. Hehre, *J. Comput. Chem.* **1987**, *8*, 861.

[40] A computed $\langle S^2 \rangle$ value for the coordinatively saturated diiron complex in the broken-symmetry singlet state is 2.07. In general, broken-symmetry calculations are significantly spin-contaminated, but spin contamination is a necessary condition for broken-symmetry calculations. If a broken-symmetry wave function has no spin contamination, we obtain the symmetric one, the spin-restricted solution.

[41] Single-point energy calculations were carried out at the B3LYP level of theory by use of TZV on all CHNO atoms of the coordinatively saturated diiron complexes optimized at the B3LYP/(TZV + 3–21G) level of theory. According to the single-point energy calculations, the coordinatively saturated diiron complex in the broken-symmetry singlet state lies 10.2 kcal mol^{-1} above that in the nonet state.

[42] a) J. P. Perdew, Y. Wang, *Phys. Rev. B* **1992**, *45*, 13244; b) J. P. Perdew, K. Burke, Y. Wang, *Phys. Rev. B* **1996**, *54*, 16533.
[43] a) D. Harris, G. L. Loew, A. Komornicki, *J. Phys. Chem. A* **1997**, *101*, 3959; b) H. Paulsen, L. Duelund, H. Winkler, H. Toftlund, A. X. Trautwein, *Inorg. Chem.* **2001**, *40*, 2201.
[44] A computed $\langle S^2 \rangle$ value for the coordinatively unsaturated diiron complex in the broken-symmetry singlet state is 2.08. The J value for this complex can be calculated (by using the following equation) to be $-66\ cm^{-1}$: $J = -(E_{HS} - E_{BS})/(4\ S_A S_B)$.
[45] K. Yoshizawa, R. Hoffmann, *Inorg. Chem.* **1996**, *35*, 2409.
[46] K. Yoshizawa, T. Yamabe, R. Hoffmann, *New. J. Chem.* **1997**, *21*, 151.
[47] D. A. Whittington, A. C. Rosenzweig, C. A. Frederick, S. J. Lippard, *Biochemistry* **2001**, *40*, 3476.
[48] D. A. Whittington, M. H. Sazinsky, S. J. Lippard, *J. Am. Chem. Soc.* **2001**, *123*, 1794.
[49] K. Yoshizawa, A. Suzuki, T. Yamabe, *J. Am. Chem. Soc.* **1999**, *121*, 5266.
[50] a) R. Hoffmann, R. W. Alder, C. F. Wilcox Jr., *J. Am. Chem. Soc.* **1970**, *92*, 4992; b) J. B. Collins, J. D. Dill, E. D. Jemmis, Y. Apeloig, P. v. R. Schleyer, R. Seegger, J. A. Pople, *J. Am. Chem. Soc.* **1976**, *98*, 5419; c) M.-B. Krogh-Jespersen, J. Chandrasekhar, E.-U. Würthwein, J. B. Collins, P. v. R. Schleyer, *J. Am. Chem. Soc.* **1980**, *102*, 2263; d) M. S. Gordon, M. W. Schmidt, *J. Am. Chem. Soc.* **1993**, *115*, 7486.
[51] E. Wigner, *Z. Phys. Chem. B* **1932**, *19*, 203.

Received: July 22, 2002
Revised: January 2, 2003 [F4269]